CONF-970517--6

SAND97-0082C
SAND--97-0082C

OXIDE FILM FORMATION FROM ELECTRON CYCLOTRON RESONANCE (ECR) PLASMAS

J. C. Barbour*, C. A. Apblett*, D. R. Denison†, and J. P. Sullivan*
*Sandia National Laboratories, Albuquerque, NM 87185-1056
†Lam Research Corporation, Fremont, CA 94538

ABSTRACT

The formation of SiO_x films and fluorine-doped SiO_x films using electron cyclotron resonance (ECR) plasma deposition is described. Parametric studies of the film composition and hydrogen content as a function of feed gas composition and RF biasing are presented. By replacing SiH_4 with SiF_4 in the gas feed, samples with F content from 2 at.% F to 12 at.% F are deposited, and the dielectric constant of the deposited layers decrease linearly with increasing fluorine concentration. The stability of these low dielectric constant SiO_xF_y layers is examined under hydrating conditions, and conditions typically found for interlayer dielectric processing in microelectronics. The hydrogen content of the SiO_2 and F-doped SiO_2 is characterized as a function of deposition conditions, and a model is given to describe the thermal release of H from SiO_2.

INTRODUCTION

The low temperature ($\leq 400°C$) deposition of silicon oxide films is important for both electronic and optical devices. The quality of the films depends on close control of the deposition parameters, and for some application the use of a high-density plasma to assist in the growth can yield superior results in comparison to thermal growth of the films. An overview will be given of the formation and properties of SiO_2 and fluorine-doped SiO_2 films formed using electron cyclotron resonance (ECR) plasmas in which feed-gas composition, sample temperature, and bias are varied. Today, the primary use of ECR deposited oxides is for filling trenches, planarization, and interlevel isolation. In recent years, the ECR deposition of SiO_2 has been extended to the formation of low dielectric constant (ε_r) interlevel dielectrics, such as fluorine-doped SiO_2, which are needed in next generation devices to reduce power consumption and RC time constants. The focus of this paper will be to examine the variation in composition and bonding for ECR-deposited films as a function of the deposition parameters given above, and then develop an empirical model to characterize the thermal release of hydrogen from the ECR-deposited silicon oxide films. The behavior of H in these materials is important because it can modify the electrical, optical, and mechanical properties. Finally, we will review the progress to date and technical challenges remaining in the development of ECR-deposited interlevel dielectrics (ILDs).

DISCLAIMER

Several studies [1-4] have characterized the ECR deposition of silicon oxide films for use in filling trenches, and in general these studies have found that holes with aspect ratios (depth/hole diameter) of up to 3 can be filled and can lead to good planarization. An RF bias is applied to the substrate during deposition in order to form a film which more closely resembles a thermal oxide in its HF etching characteristics. Also, the RF bias causes sputtering of the film at the top of the hole during the deposition process. This sputtering of the SiO_2 film at the top and near the edge of the via allows for filling of the via without pinching-off the hole. Shadowing effects, during deposition in a via, are also eliminated by use of a mirror magnetic field distribution to shape the plasma in the region of the sample for a more uniform plasma with ions incident normal to the substrate surface.

A challenge which still remains with the ECR plasma deposition is control of the plasma damage to gate oxides below the ILD layer. This damage is a result [5,6] of high currents of electrons flowing into the gate region during the deposition of the ILD layer. This excess charging of the gate can then lead to breakdown of the gate oxide. Excess charging of the gate can be reduced by controlling the flux of electrons reaching the substrate by reducing the microwave power and magnetic field density in the region of the sample. Bothra et al. [5] showed that the leakage current for 9.0 nm gate oxides could be reduced sufficiently by keeping the microwave power $\leq$ 1900 Watts and by using a magnetic field distribution in a cusp geometry rather than a mirror geometry. Further studies will be required in the future to determine the effects of plasma charging on thinner gate oxides which will be used in future generation devices. In this paper, the range of microwave powers used for depositing films was 1600-1800 Watts.

EXPERIMENT

An important aspect for all ILD layers is the effect that hydrogen incorporation can have on the electronic and mechanical properties. The H content in as-deposited films depends on the temperature and bias during deposition, and on the stoichiometry of the films. In this experiment, we have manipulated the deposition parameters to study the variation in composition and H content, and then used post-deposition thermal annealing treatments to control the uptake and release of hydrogen from the films.

A schematic drawing of a Lam EPIC ECR plasma deposition reactor is shown in fig. 1 along with the range of parameters used in this study. Microwaves of frequency 2.45 GHz were guided using a 1/4 wave-1/2 wave guide and introduced into the top of the reactor through a cooled quartz window. A power of 1600 W was used for the deposition of SiO_2 and a power of 1800 W was used for the deposition of SiO_xF_y. The microwaves enter a quartz bell jar (denoted plasma chamber in fig. 1) surrounded by concentric DC electromagnets which can produce a magnetic field in excess of 1000 G in the plasma chamber. For a frequency of 2.45 GHz, the resonance condition is established at the point where the magnetic field is 875 G which is inside the plasma chamber and 24.5 cm from the sample. The wafers were held by an electrostatic chuck in a chamber

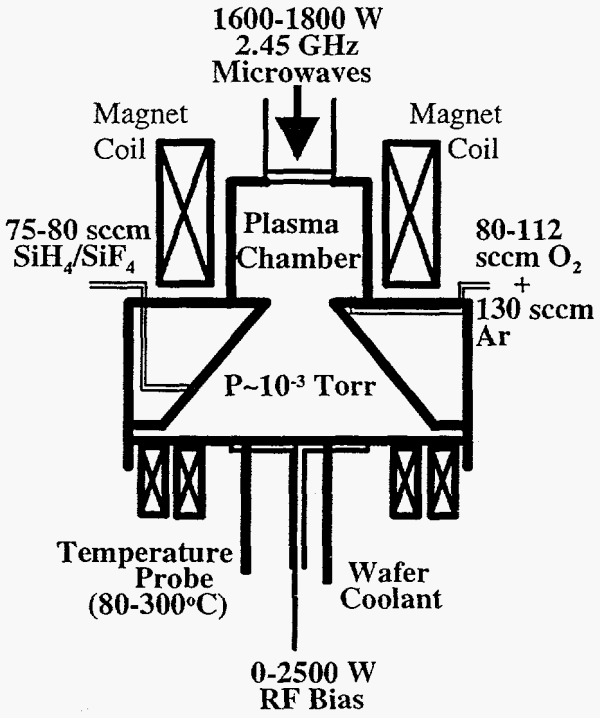

Fig. 1. Schematic drawing of ECR apparatus used to deposit SiO_2 and fluorine-doped SiO_2. The range of deposition conditions examined in this paper are as shown.

downstream from the plasma chamber. Two downstream magnets were located directly under the chuck and were used to shape the magnetic fields into a mirror configuration.

Both Ar and O_2 gas were injected at the bottom of the plasma chamber. The Ar was more easily ionized and thereby helped to ionize the oxygen in the plasma. For SiO_2 films, the flow of Ar was held constant at 130 sccm while the O_2 flow was varied from 80 to 112 sccm to study the change in film composition with variation in gas feed stoichiometry. The O_2 gas flow for the deposition of SiO_xF_y films was 112 sccm. Neutral molecules and energetic ions stream down onto the sample in the downstream chamber and react with SiH_4 near the sample. Silane was introduced into the sample chamber just above the sample position. The SiH_4 gas flow was held constant at 75 sccm to make the SiO_2 films, while a mixture of SiH_4 and SiF_4 was introduced at a fixed flow rate for the combined gases of 80 sccm to make the F-doped films. The $SiF_4/(SiH_4+SiF_4)$ gas ratio was varied from 0 to 0.9 in order to vary the level of fluorine doping. The pressure in the sample chamber was $\approx 2x10^{-3}$ Torr during the depositions.

Energetic ion effects on the SiO_2 film properties were examined by applying a 13.56 MHz RF bias to the electrostatic chuck. The samples were biased using 0 to 2500 W of RF power. The chuck was temperature controlled to 75°C by water channels within the metal plate, and plasma heating of the samples was controlled by adjusting the heat loss out of the back of the wafer to the chuck. To enhance the heat exchange between the wafer and the chuck, a static pressure of helium was used as a wafer coolant in the waffle channels between the back of the wafer and the chuck surface, resulting in enhanced thermal contact. Temperature control of the wafer surface from 80-300°C was achieved by adjusting the static pressure of helium gas, thus adjusting the rate at which heat lost from the wafer could flow to the chuck. A single point optical probe was used to monitor the wafer temperature.

The compositions of the samples were measured using several ion-beam analysis techniques [7,8], and the bonding configurations were characterized using Fourier

transform infra-red spectroscopy (FTIR). The Si and O compositions were determined using 2.8 MeV He^+ Rutherford backscattering spectrometry (RBS) with a scattering angle of 164°. The hydrogen content was determined using 16-30 MeV Si ion elastic recoil detection (ERD) with an incident angle of 75° from the sample normal and a scattering angle of 30°. Different energies were used in the ERD measurements depending upon the film thickness. Nuclear reaction analysis (NRA), using ≥ 872 keV incident protons while detecting 6.13, 6.72, and 7.12 MeV emitted γ-rays, was done to determine the concentration of F in the F-doped SiO_2. In order to determine the energy for thermal release of H, samples were isochronally annealed for 15 min. in a vacuum of $1x10^{-8}$ to $1x10^{-7}$ Torr. Hydration of SiO_xF_y films was performed by boiling these samples in distilled H_2O for one hour (95°C at 690 Torr). The dielectric constant of the SiO_xF_y films was determined by depositing the layers on Al/Si substrates and then measuring the capacitance from a metal-insulator-metal structure.

RESULTS AND DISCUSSION

The following sections describe: the effects of energetic ions on film formation, the control of composition with variation in gas feed for both SiO_2 and F-doped SiO_2, the energy for thermal release of H from SiO_2, and then the formation of and technical problems to be addressed in the formation of low dielectric constant SiO_xF_y ILD layers. Typical processes for ECR deposition of ILD layers employ an RF bias to achieve good gap fill and planarization, and thus these processes have been optimized for the case of an applied RF bias. In the next section, we will describe the effects that the bias has on the formation of SiO_2 layers.

Energetic Ion Beam Effects

The first effect found with the application of an RF bias is an increase in the sample temperature. A sample deposited without an applied bias (using a wafer coolant pressure of 6 Torr) reaches a temperature of 80°C during the deposition, whereas a sample deposited with an RF bias of 1140 W (using a wafer coolant pressure of 12 Torr) reaches a temperature of 280°C. This increase in temperature is a result of the increased flux of energetic particles impinging upon the sample. A sample in an unbiased ECR plasma has ions incident with an energy of ≈ 30 eV while the application of an RF bias increases the ion energy to ~100 eV. This increase in ion energy also causes a competition between deposition and sputtering of the film which results in a thinner layer for the film deposited with an applied bias in comparison to that deposited without an applied bias. Figure 2 shows the Si and O composition depth profiles for two samples, both deposited for a total of 123 sec: one deposited with an applied RF bias of 1140 W (dashed line for the Si profile and x for the O profile), and the other deposited without an applied bias (solid line for the Si profile and o for the O profile). The sample deposited using the RF bias is approximately 530 nm thick, while the sample deposited without an RF bias is approximately 740 nm thick.

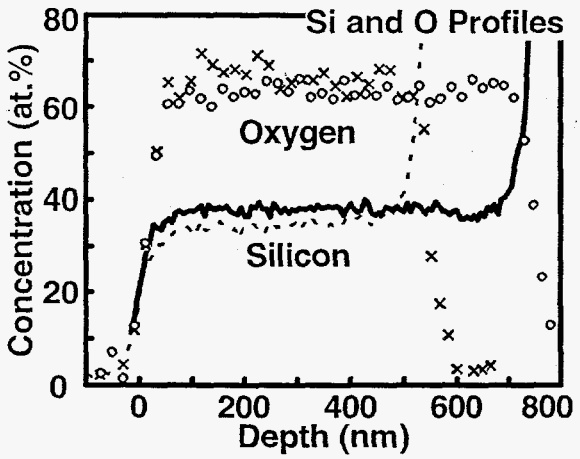

Fig. 2. Si and O composition depth profiles determined using RBS analysis of samples deposited with and without an RF bias.

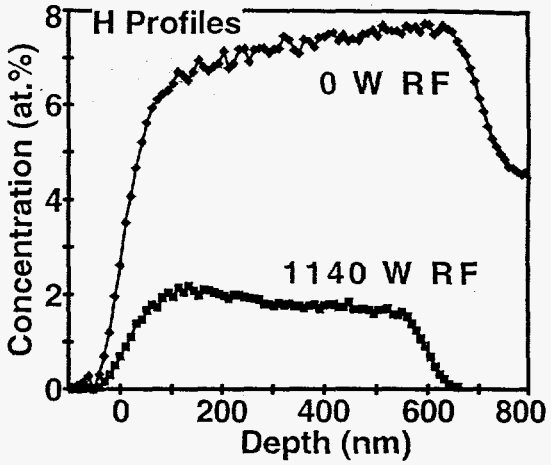

Fig. 3. Hydrogen composition depth profiles determined using ERD analysis of the same samples as measured in fig. 1.

Further, the sample deposited with an RF bias has an O/Si ratio of 2 and an index of refraction of 1.46, while the sample deposited without an RF bias has an O/Si ratio of .1.7 and a higher index of refraction due to the excess Si. Also, the application of a bias pulls more Ar from the plasma into the film and increases the Ar content from 0.3 at.% (sample without a bias) to 0.6 at.% (sample with a bias). Figure 3 shows the composition depth profiles of H in these two samples in which the RF bias causes the sample to have a lower H concentration by a factor of 3.5. This decreased hydrogen content can be attributed to: a composition which is closer to stoichiometric SiO_2, the higher deposition temperature, or a denser film formed with the energetic ions. Thus, the use of energetic ions during deposition can not only cause sputtering of the film, but significantly alters its composition. All of the samples examined in the remainder of this paper were deposited with an applied RF bias (1400 W for SiO_2 samples and 2500 W for SiO_xF_y samples).

Control of Composition with Variation in Gas Feed

In this section, we will examine the change in the SiO_2 composition as a function of increasing ratio of O_2 to SiH_4 in the gas feed. For this set of samples, the SiH_4 gas flow was fixed at 75 sccm while the O_2 gas flow was increased from 80 sccm to 112 sccm. The RF power was held fixed at 1400 W and the sample temperature was held approximately constant at 260-300°C. Figure 4 shows that as the deposition chemistry is changed from an oxygen starved condition to an oxygen rich condition the O/Si ratio increases to 2 (open circles) while the index of refraction (n) decreases to 1.46. Similar to the results stated above, the excess Si increases n well above 1.46 which is the value normally found for SiO_2. The hydrogen content for these films also shows a variation with the O_2 feed gas flow, although this variation is not quite as systematic as for n. The

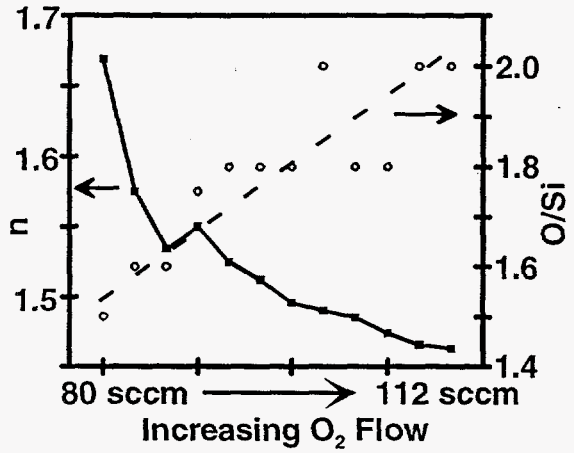

Fig. 4. Variation in index of refraction (solid line) and composition of the deposited film (O/Si ratio = open circles) as a function of increasing O_2 flow in the gas feed. The dashed line is drawn to help guide the eye.

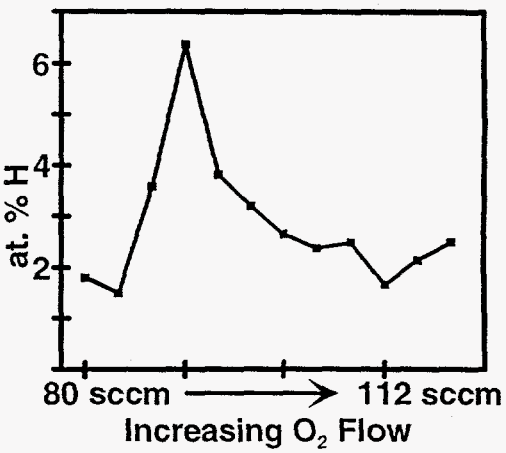

Fig. 5. Variation in hydrogen content as a function of increasing O_2 flow in the gas feed.

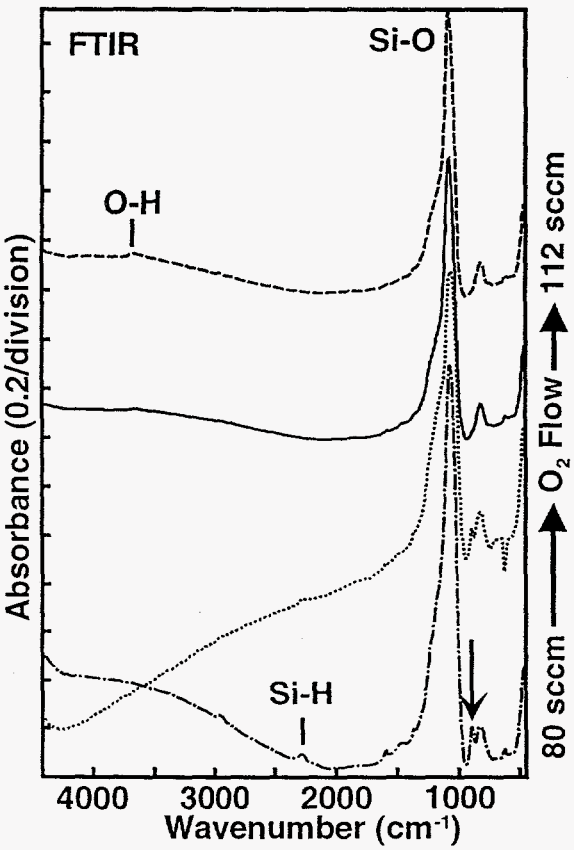

Fig .6 FTIR spectra reveal a change in the bonding within the film as the O_2 flow is increased.

concentration of H varies only slightly (between 1.7 at.% H and 2.7 at.% H) as the O/Si decreases from 2 to 1.8. The H content then increases sharply and peaks at 6.4 at.% H for an O/Si ratio of 1.7 and decreases back to 1.5-1.8 at.% H as O/Si decreases to 1.5. This peak in the concentration of H is attributed to an increase in the amount of excess Si and thereby excess Si-H bonding in the film, up to a point where the increased Si causes a significant amount of Si-Si bonding and a decrease in the H content.

A more detailed examination of the bonding of H in these SiO_2 films as a function of O/Si ratio was done using FTIR and the change in the type of bonding is shown in fig. 6. The curves are offset in the vertical direction in order to more easily identify and compare peak positions. These four spectra were taken from samples with O/Si ratios varying from 1.7 (dash-dot line at bottom) to 2 (dashed line at top), corresponding to the samples at the peak

H concentration up to an O_2 flow of 112 sccm shown in fig. 5. FTIR spectra from samples to the left of the peak in fig. 5 are not presented here because these samples deviated too far from stoichiometry. The total hydrogen content measured using ERD for these four samples was: 2.5 at.% H (top curve), 2.4 at.% H (solid line), 3.8 at.% H (dotted line), 6.4 at.% H (bottom curve). The primary peaks observed in the FTIR spectra of fig. 6 are as follows: an Si-O rocking mode at 450 cm^{-1}, a Si substrate peak at 613 cm^{-1}, an Si-H bending mode at 630-690 cm^{-1}, an Si-O bending mode at 810 cm^{-1}, Si-H_2 and SiH_3 bending modes at 880-890 cm^{-1} (indicated by an arrow in fig. 6), an Si-O stretching mode at 1070 cm^{-1}, an Si-H stretching mode at 2260 cm^{-1} (indicated by a straight line), and an O-H stretching mode at 3625-3675 cm^{-1} (indicated by a straight line). This figure shows that the attachment of H in ECR-deposited SiO_2 changes from O-H type bonds to Si-H, Si-H_2, and Si-H_3 as the deposition chemistry is changed to an oxygen starved condition. Therefore, not only the total H content, but the types of bonds formed for H trapping in SiO_2 are expected to be important in considering the thermal release of H.

The Energy for Thermal Release of H from SiO_2

Previously, the thermal release of H from ECR-deposited Si_3N_4 films was characterized [9] and a distributed trap energy model was developed [10] to determine the average energy for release of hydrogen. The model accurately described the energetics for the thermal stability of H and predicted the release of H from three type of trapping sites in Si_3N_4 with different trap energies: Si-H bonds with a trap energy of 3.30 eV, and two types of N-H bonds with trap energies of 3.34 eV and 4.05 eV. The average (or effective) thermal release energy, $E_{effective}$, was given as the weighted average of the

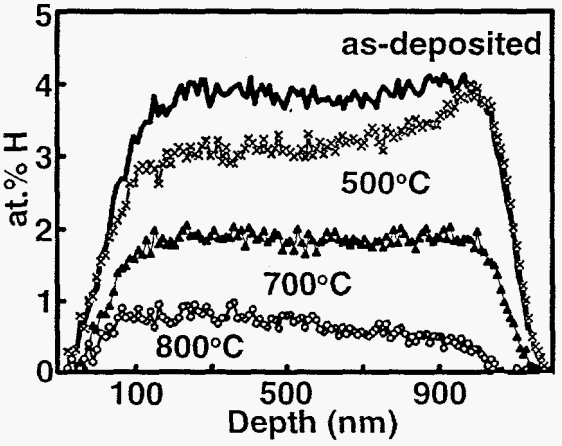

Fig. 7. Concentration depth profiles for H in a series of samples (O/Si=1.8) which were vacuum annealed for 15 min. each at the temperatures indicated.

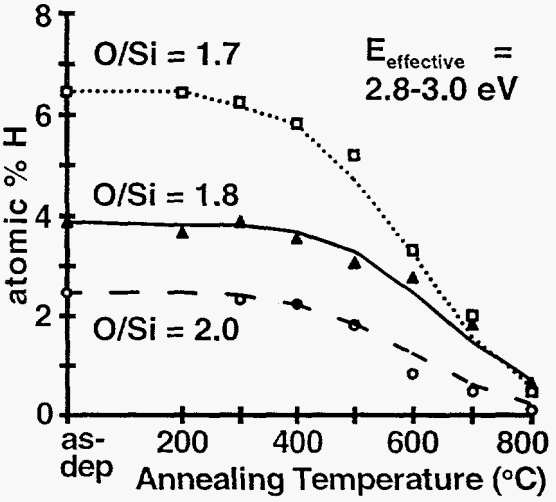

Fig. 8. The effective activation energy for thermal release of H from three sets of samples with different O/Si ratios. The experimental data are shown as individual points and the fit of the model to the data are shown as lines.

separate trap energies: $E_{effective} = 3.30\ \Gamma_{Si\text{-}H} + 3.34\ \Gamma_{N1\text{-}H} + 4.05\ \Gamma_{N2\text{-}H}$ in eV, where the weighting factors, Γ, are the fractions of Si-H, N1-H, and N2-H bonds. This model will be extended in this paper to determine the effective thermal release energy of H from ECR-deposited SiO_2.

First, the annealing behavior of the SiO_2 samples with different types of H attachment within the SiO_2 matrix will be characterized, allowing a determination of the temperature at which the H begins to be released. Then this thermal release behavior will be modeled to determine $E_{effective}$. The hydrogen concentration depth profiles for the set of O/Si=1.8 samples, after vacuum annealing, is shown in fig. 7. The samples were annealed each for 15 min. at different temperatures from 100°C to 800°C in increments of 100°C. The H profiles for the samples annealed ≤300°C did not differ from the profile for the as-deposited sample. A small amount of hydrogen was released at 400°C with increasing amounts of hydrogen released for each of the higher annealing temperatures. All of these profiles are relatively constant with depth, demonstrating that the H releases and diffuses quickly through the entire ≈1.1 μm thick sample in 15 min. The diffusion of hydrogen species in SiO_2 is known to be extremely rapid [11,12] if retrapping is negligible. The diffusivities of ^2H and $^2H_2$ in SiO_2 at 100°C are $4x10^{-7}$ cm^2/s and $3x10^{-10}$ cm^2/s, respectively. Further, annealing of the SiO_2 can cause densification of the film and anneal-out dangling bonds left by the H release. Therefore, retrapping of H will be neglected to first order, but experiments measuring the release of H as a function of time at a given temperature will be examined below to check the validity of this assumption.

Figure 8 shows the experimentally determined total hydrogen concentrations as a function of annealing temperature for three types of samples with differing O/Si ratios: ■ for O/Si = 1.7, ▲ for O/Si = 1.8, and ● for O/Si = 2.0. The data are given for the concentration at 1/2 the total depth of the sample and are shown as individual data points. The lines (dotted, solid, and dashed) are determined for each of these samples using the initial, as-deposited H concentration and the effective activation energy in the model described below. This figure shows that although the oxygen deficient samples have a higher hydrogen content, the onset temperature for release of hydrogen from all of these samples is approximately the same, as is the energy for thermal release.

For a single trap energy, the probability (Π) of H thermally escaping a trap at an annealing temperature T is given by an attempt frequency times a Boltzmann factor: $\nu \exp(-E_B/kT)$, where ν is the order of 10^{13} s^{-1} for thermal vibrations. After having filled the traps to saturation (assumed to occur during deposition and supported by the fact that annealing below the deposition temperature does not alter the H concentration), the release of H from a trap with energy E_B is governed by a first order rate equation in which the concentration of H in traps at time t is: $d[H]/dt = -\Pi\ [H]$. The solution to this equation for the i^{th} trap is: $[H(T)]_i = [H_o(T)]_i \exp(-\nu\ t \exp(-E_{Bi}/kT))$, where $[H_o(T)]$ is the initial H concentration before annealing at temperature T. For negligible trap interaction

and negligible retrapping, the total concentration of H is the sum over the energy-distribution for the traps: atomic $\%H = \Sigma_i [H_i] = \Sigma_i [H_o]_i \exp(-\nu\, t \exp(-E_{Bi}/kT))$ (1).

If a single energy was considered for E_B in equation (1), then the curves for the total release of H as a function of annealing temperature appears as step functions in which nearly all of the H is released at one temperature. Therefore, a Gaussian distribution of nine trap energies centered around $E_{effective}$ was used to represent the possible distribution of bonds, angles, and state of relaxation of the amorphous SiO_x films. The standard deviation of the distribution, σ=0.5 eV, was minimized to obtain a good fit to the data. The effect of σ was to help round the curves of fig. 8 but it did not alter their inflection points or the values determined for $E_{effective}$. Thus, the effective activation energy for thermal release of H was determined by fitting equation (1) to the data using the measured initial H concentration and t=900 s. The $E_{effective}$ determined for the top and bottom curves in fig. 8 was 2.8 eV, and $E_{effective}$ determined for the middle curve was 3.0 eV. This range of activation energies is close to the Si-D bond energy (2.85 eV) measured by Myers and Richards [13] for D trapped in ion irradiated thermal oxides. Their measurement for the O-D bond energy was 3.16 eV. $E_{effective}$ is an average of the release energy for the different types of H trapping sites in the ECR-deposited SiO_2. Since the same value of $E_{effective}$ was determined for the samples with predominantly O-H bonding as for the sample with predominantly Si-H bonding, then the binding energy for O-H in the ECR oxides appears to be similar to the binding energy for Si-H and approximately equal to 2.9 eV. A difference in O-H binding energy between ECR oxides and thermal oxides may result from a slight difference in density and stress state, but the effects of kinetically limited H retrapping on the determination of $E_{effective}$ should be examined.

The validity of the assumptions used in the model given above were checked by performing experiments to measure the kinetics of the H release and loss from the sample at two annealing temperatures: 500°C for 675 min. and 600°C for 495 min. These times were chosen to increase the possible effective diffusion distance by more than a factor of 5, if a diffusion limited process was predominant. Figure 9 shows that further loss of H with extended annealing can occur, although the amount of loss is small. The H profile after extended annealing is still relatively constant throughout the film. Moreover, the data for the extended anneals shown as open squares in fig. 10 can still be fit well with an activation energy of 3.0 eV (model shown as open triangles). The fit to the data was done using equation (1) with σ=0.5 eV and with the respective times for the longer annealing treatments. (Since different annealing times were used, the lines drawn through the open squares and triangles in fig. 10 are drawn to guide the eye.) Equation (1) shows that the dependence on time in determining the effective activation energy for thermal release of H from ECR-deposited oxides is smaller than the dependence on temperature, and therefore the value of $E_{effective}$ is changed very little by using longer annealing times.

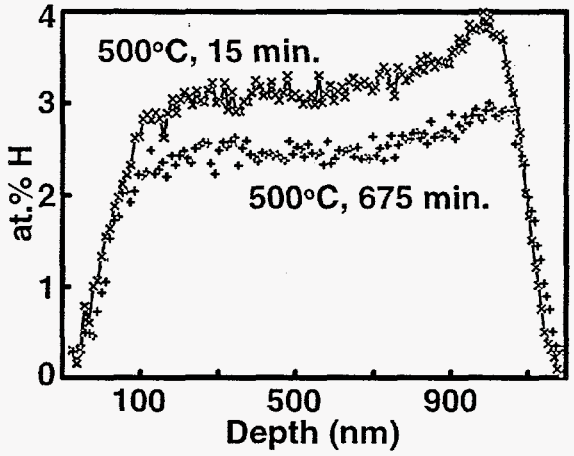

Fig. 9 Concentration depth profiles for H in the O/Si=1.8 sample which was annealed for 675 min. at 500°C to check the effects of kinetics on determining the release energy.

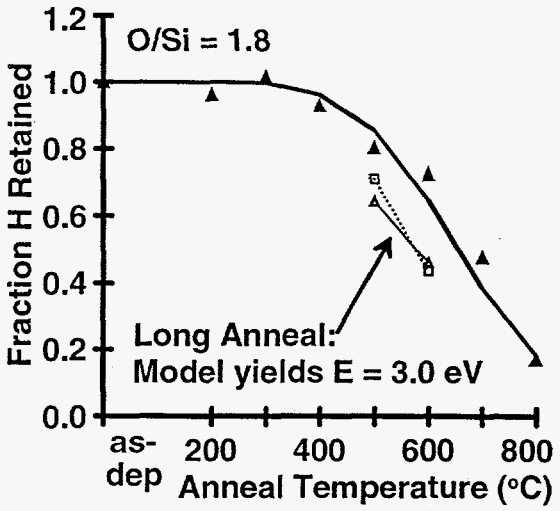

Fig. 10. The effective activation energy for thermal release of H from the O/Si= 1.8 samples annealed for extended times at 500°C and 600°C are shown in addition to data for 15 min. annealing times (▲).

Low Dielectric Constant SiO_xF_y

Fluorine-doped SiO_2 is being investigated widely throughout the world [8, 14-18] as a replacement for SiO_2 ILDs in future generation microelectronics. Moreover, ECR plasma deposition of SiO_xF_y films is of great interest because these films tend to show improved degradation resistance in the presence of moisture in comparison to other deposition techniques. This section will review the results to date in the ECR formation of low ε_r SiO_2 films and then examine the technical problems which must still be addressed for integration of these films into microelectronic processing. For example, Chang et al. [16] found that the thermal stability of F and moisture resistance are greatly improved by increasing the deposition temperature, but at the same time the compressive stress and ε_r are both increased.

A parametric study was done to measure the change in composition, dielectric constant, and stress of SiO_xF_y as a function of increasing the gas-feed ratio $SiF_4/(SiH_4+SiF_4)$ from 0 to 0.9. For this set of samples, the combined SiH_4+SiF_4 gas flow was fixed at 80 sccm. The O_2 gas flow was fixed at 112 sccm. The RF power was 2500 W and the sample temperature was held approximately constant at 300°C. Figure 11 shows that as the deposition chemistry is changed from SiH_4-rich to SiF_4-rich, the concentration of Si (◇) in the film remains constant, but the concentration of O (●) decreases steadily while concentration of F (+) increases steadily to 10.3 at.% F. Simultaneously, the H content is decreased to 1.1 at.% H and the film stress becomes less compressive (66 MPa) with increasing F content (not shown). Figure 12 shows that ε_r

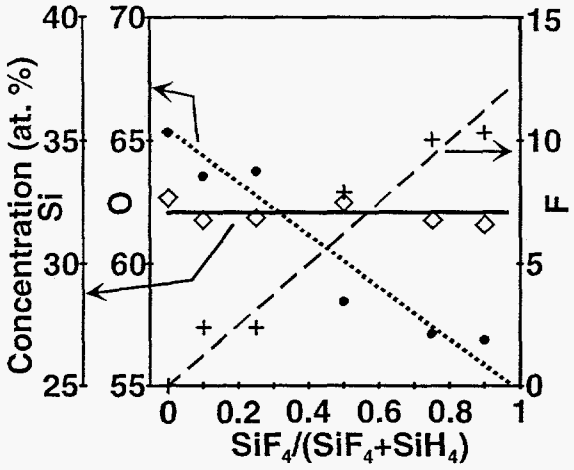

Fig. 11. Variation in film composition with increasing SiF_4 content in the feed gas. The data points are as follows: Si=◇, O=●, and F=+. The lines are drawn to guide the eye.

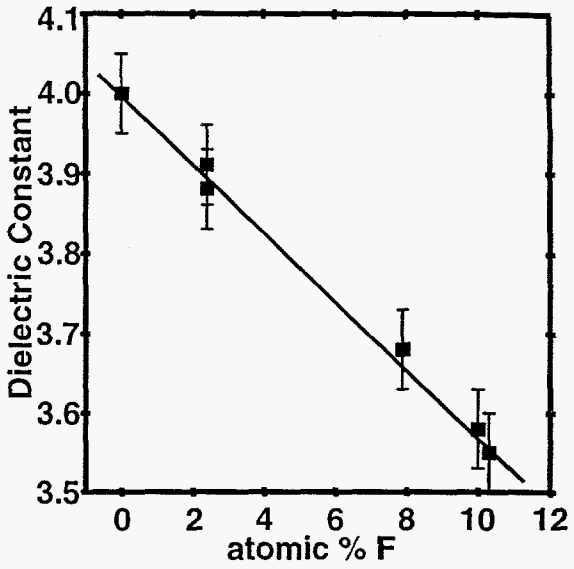

Fig. 12. Variation in the dielectric constant with increasing F concentration. Fluorine concentrations greater than 13 at.% were not obtained.

decreases linearly with increasing F content, from 4.0 for the undoped SiO_2 to 3.55 for the film containing 10.3 at.% F. A film with a fluorine concentration as high as 12.2 at.% F has been deposited, but the dielectric constant has not yet been measured in the metal-insulator-metal structure. Thus, the addition of F into the feed gas increases the F content in the film which decreases the stress and ε_r to a value which is expected to be slightly less than 3.5.

Although ε_r decreases with the addition of F to SiO_2, the mechanical stability and stability of ε_r when annealed or exposed to a humid environment still present barriers to be overcome for the integration of SiO_xF_y films into microelectronic processes. Sullivan et al. [18] found two types of thermal instability for SiO_xF_y films. One instability which increased with increasing F content was related to the absorption of moisture. This absorption was independent of the type of substrate (Si, Al/Si, TiN/Al/Si, or Al/SiO_2/Si). However, the other instability associated with a loss of F from the film was dependent upon the type of substrate and occurred when films on Al/Si substrates were hydrated and annealed at 400°C. This annealing temperature should be sufficient to release trapped water from the sample, but as shown in the previous section, 400°C is insufficient temperature to greatly change the level of SiO-H and Si-H in these samples. Therefore, a characterization of the uptake and release of moisture from these SiO_xF_y films is important. It was suggested that the use of a moisture barrier such as TiN could eliminate these instability problems.

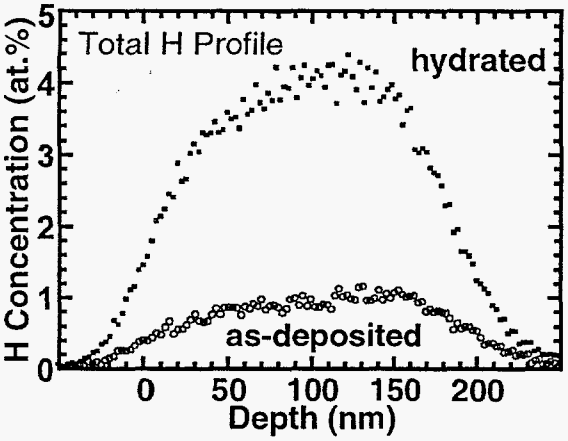

Fig. 13. Concentration depth profiles of H in a sample containing 11 at.% F, before and after hydration in boiling water.

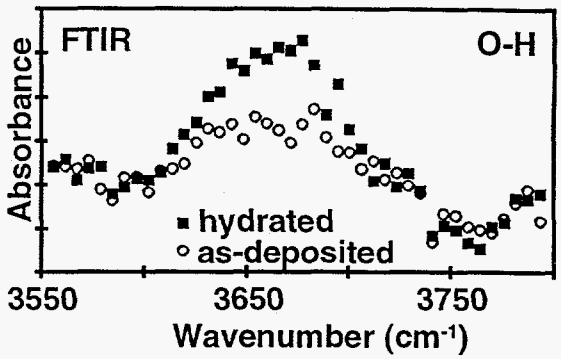

Fig. 14. The O-H stretching mode peak in FTIR spectra from a sample containing 11 at.% F, measured before and after hydration in boiling water

Several samples with a range of F content from 2 at.% F to 11 at.% F were hydrated in boiling water and the level of H was then measured using ERD and FTIR. As stated above, the largest uptake in moisture was observed for the higher F content samples. The total H concentration determined from ERD analysis for the 11 at.% F sample before and after hydration is shown in fig. 13, and the O-H content determined using FTIR from a similar sample is shown in fig. 14. The total H content increased by a factor of 4. The Si-H signal in the FTIR spectra (not shown) was unchanged after hydration, while the O-H signal increased by only a factor of 2. The O-H signal remained the same after a 400°C vacuum anneal. These results imply that the excess hydrogen in the sample which appears in the ERD spectra are trapped in the sample as H_2O and appear as a broad peak in the FTIR spectra which is only visible as part of the background signal. This trapped H can weaken the mechanical integrity of the SiO_xF_y film or other films deposited on top of the SiO_xF_y. In addition, the problem with moisture absorption appears in samples exposed to air for extended times as well as samples treated in boiling water. A 1 μm thick SiO_xF_y film deposited on Si with 10.3 at.% F was left uncapped and exposed to the laboratory air for more than a year and then analyzed using ERD. Excess H was found in this air exposed sample as shown in fig. 15. The sample was then

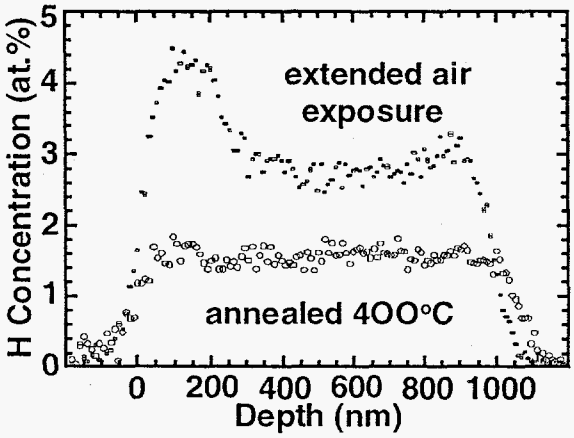

Fig. 15. H concentration depth profile for an 11 at.% F sample exposed to air for more than one year (top) and then vacuum annealed at 400°C (bottom).

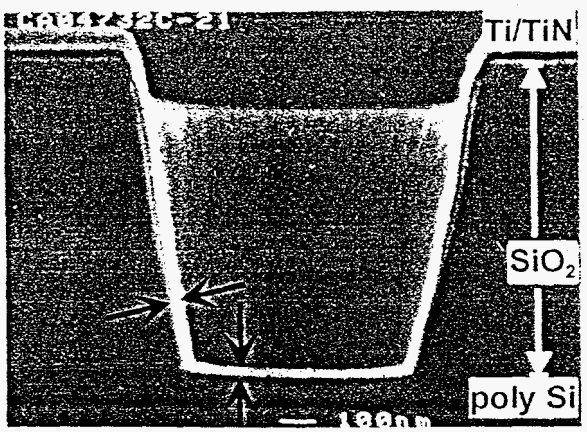

Fig. 16a. SEM micrograph showing the adhesion of a Ti/TiN layer inside a via cut through an ECR-deposited SiO_2 film. The black arrows indicate the thickness of the Ti/TiN layer on the sidewalls and bottom of the via.

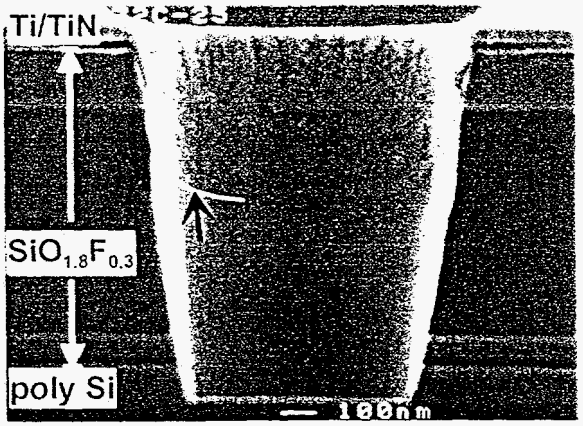

Fig. 16b. SEM micrograph showing the adhesion of a Ti/TiN layer inside a similar via cut through a $SiO_{1.8}F_{0.3}$ layer. The black arrow indicates a region of the TiN layer which detached and is hanging free in the via. A white line was drawn along the bottom of this free-hanging layer.

vacuum annealed at 400°C, a temperature where the loss of Si-H and O-H is negligible but the loss of water is significant, and the sample was re-analyzed. This annealing treatment decreased the total H content by a factor of 2. Therefore, some type of moisture barrier will be required to protect the SiO_xF_y ILD layer in microelectronic applications.

As stated above, TiN is one possible barrier which works well for planar applications. Typically, a thin Ti adhesion layer is deposited followed by deposition of TiN, but this type of configuration does not work well when coating the inside of vias through SiO_xF_y as shown in the comparison of figs. 16a and 16b. The sample shown in fig. 16a was made by etching a via through the SiO_2 layer followed by sputter deposition of a Ti/TiN layer onto the top surface and into the via. The TiN liner forms a uniform continuous film on the sidewalls and bottom of the via as indicated with the black arrows. (The polycrystalline Si layer where the Ti/TiN contact the bottom of the via would typically be a titanium silicide contact layer, but for the purposes of these test structures, a polycrystalline Si layer was used instead.) In contrast, fig. 16b shows that for the same etching process the fluorinated ILD layer was etched more severely and the bottom polycrystalline layer was then attacked. This effect can be easily taken into account in future etching operations, but more importantly for the fluorinated SiO_2, the Ti/TiN layer de-adheres from sidewalls in the ILD via. The Ti/TiN liner remains on only the top third of the contact. This deadhesion behavior is probably a result of moisture absorption as described above, and therefore a 400°C annealing treatment may be needed prior to sputter deposition in order to drive-off excess moisture in the ILD layer. As SiO_xF_y films find use in microelectronic applications, further process development will likely be encountered for many of the conventional steps currently used with SiO_2 ILD processing.

CONCLUSIONS

The primary mechanism to control film composition for ECR-deposited oxides is by adjustment of the gas-feed composition. The O/Si and F/Si concentration are directly proportional to gas flows. However, the H content is more dependent upon other factors which can influence the bonding in the film and the density of the film. These factors include the sample bias, the sample temperature, and the amount of deviation from a stoichiometric SiO_2 film composition. A Si-rich film will have a higher H content and exhibit H-attachment primarily to Si rather than O, whereas a stoichiometric SiO_2 film has most of the H trapped in O-H bonds.

By varying the composition of the SiO_2 films (including the hydrogen content), the electrical, optical and mechanical properties can be changed extensively. The most dramatic change is through the use of fluorine doping in order to decrease the dielectric constant. The dielectric constant of SiO_xF_y can be decreased to below 3.5 by increasing the fluorine composition to 11-12 at.%, but at the same time, the film stability decreases. The stability of the fluorinated SiO_2 can be increased through annealing treatments and through the use of capping layers (such as SiO_2 and TiN), but these additional processes may also act to increase the dielectric constant of the SiO_xF_y layer or combined layers.

Ion irradiation during deposition of the SiO_2 was shown to modify the film formation by sputtering which produced a thinner film but one with fewer weakly bound species, and by densification which reduced hydrogen content.

Finally, the release of hydrogen from both ECR deposited oxides and nitrides was well characterized by an empirical distributed-trap-energy model using an equation of the form: $\%H = \Sigma_i [H_i] = \Sigma_i [H_o]_i \exp(-\nu\, t \exp(-E_{Bi}/kT))$, where the i^{th} trap has binding energy E_{Bi}, and the initial concentration of hydrogen before annealing is H_o. Thus, by knowing only the initial hydrogen concentration in a film and the binding energies for Si-H and O-H in the film, the thermal annealing behavior of SiO_2 films can be predicted using this model. The effective activation energy for the thermal release of H from ECR-deposited SiO_2 was determined to be 2.8-3.0 eV, and the temperature for significant release of H from SiO_2 is > 400°C.

ACKNOWLEDGMENTS

The authors would like to thank Dan Buller for his assistance in performing the ion beam analysis. Sandia is a multiprogram laboratory operated by Sandia Corporation, a Lockheed Martin Company, for the United States Department of Energy under contract DE-AC04-94AL85000. This work was funded by: the Office of Basic Energy Sciences (Division of Materials Sciences / Metals and Ceramics), a Cooperative Research and Development Agreement with LAM Research Corporation, and a Laboratory Directed Research and Development Program.

REFERENCES

[1] S. V. Nguyen and K. Albaugh, J. Electrochem. Soc. 136, 2835 (1989).

[2] R. G. Andosca, W. J. Varhue, and E. Adams, J. Appl. Phys. 72, 1126 (1992).

[3] K. Machida, C. Hashimoto, and H. Oikawa, J. Vac. Sci, Technol. B 11, 224 (1993).

[4] C. S. Pai, J. F. Miner, and P. D. Foo, J. Appl. Phys. 73, 3531 (1993).

[5] S. Bothra, C. T. Gabriel, S. Lassig, and D. Pirkle, J. Electrochem. Soc. 142, L208 (1995).

[6] K. Machida, M. Itsumi, K. Minegishi, and E. Arai, J. Vac. Sci. Technol. B 13, 2004 (1995).

[7] For example, see Handbook of Modern Ion Beam Materials Analysis, edited by J. R. Tesmer, M. Nastasi, J. C. Barbour, C. J. Maggiore, and J. W. Mayer (Materials Research Society, Pittsburgh, 1995) 704 pp.

[8] J. H. Burkhart, D. R. Denison, J. C. Barbour, and C. A. Apblett, Nucl. Instrum. Methods B 118, 698 (1996).

[9] J. C. Barbour and H. J. Stein, in Photons and Low Energy Particles in Surface Processing, edited by C. I. H. Ashby, J. H. Brannon, and S. W. Pang (Materials Research Society, Pittsburgh, 1992), vol. 236, p. 313.

[10]J. C. Barbour, in Silicon Nitride and Silicon Dioxide Thin Insulating Films, Vik J. Kapoor and William Brown, eds. (The Electrochemical Society, Inc., Pennington, NJ, 1994) p. 505.

[11]D. L. Griscom, J. Appl. Phys. 58, 2524 (1985).

[12]J. E. Shelby, J. Appl. Phys. 48, 3387 (1977).

[13]S. M. Myers and P. M. Richards, J. Appl. Phys. 67, 4064 (1990).

[14]T. Homma, J. Non-Cryst. Solids 187, 49 (1995).

[15]T. Tamura, Y. Inoue, M. Satoh, H. Yoshitaka, and J. Sakai, Jpn. J. Appl. Phys. 35, 2526 (1996).

[16]K. M. Chang, S. W. Wang, C. J. Wu, T. H. Yeh, C. H. Li, and J. Y. Yang, Appl. Phys. Lett. 69, 1238 (1996)

[17]S. Lee and J.-W. Park, J. Appl. Phys. 80, 5260 (1996).

[18]J. P. Sullivan, D. R. Denison, J. C. Barbour, P. P. Newcomer, C. A. Apblett, C. H. Seager, and A. G. Baca, in Low Dielectric Constant Materials, edited by A. Lagendijk, H. Treichel, and K. Uram (Materials Research Society, Pittsburgh, 1997), vol. 443, in press.